scientific reports

Check for updates

OPEN

Optomechanically induced gain using a trapped interacting Bose-Einstein condensate

H. Mikaeili[1], A. Dalafi[1]✉, M. Ghanaatshoar[1] & B. Askari[2]

We investigate the realization of the phenomenon of optomechanically induced gain in a hybrid optomechanical system consisting of an interacting Bose-Einstein condensate trapped inside the optical lattice of a cavity which is generated by an external coupling laser tuned to the red sideband of the cavity. It is shown that the system behaves as an optical transistor while the cavity is exposed to a weak input optical signal which can be amplified considerably in the cavity output if the system is in the unresolved sideband regime. Interestingly, the system has the capability to switch from the resolved to unresolved sideband regime by controlling the *s*-wave scattering frequency of atomic collisions. We show that the system gain can be enhanced considerably by controlling the *s*-wave scattering frequency as well as the coupling laser intensity while the system remains in the stable regime. Based on our obtained results, the input signal can be amplified more than 100 million percent in the system output which is much larger than those already reported in the previously proposed similar schemes.

In recent decades, ultracold atomic ensembles trapped in optical lattices generated by quantized light fields[1] and hybrid optomechanical systems containing Bose-Einstein condensates (BECs)[2–5], where the excitation of a collective mode of the trapped atoms plays the role of the vibrational mode of the moving mirror in a bare optomechanical system (OMS)[6], have attracted much attention. Such systems have been known as a good platform for studying the interaction of light with matter in the regime where their quantum mechanical properties are manifested in the same level[7–11].

The optomechanical coupling generated by an external coupling laser between the optical mode of the cavity and the fluctuation of the collective excitation of the BEC (the so-called Bogoliubov mode)[12,13], makes the system behave effectively as a two-mode quantum system in which the phenomenon of optomechanically induced transparency (OMIT)[14–17] can be observable while the cavity is also driven by another external weak probe laser. One of the most important features of a hybrid OMS containing a BEC is the nonlinear effect of atomic collisions which behaves as an atomic parametric oscillator[18–21] which brings more controllability[22,23] and can increase the quantum effects at the macroscopic level[24–26].

A remarkable feature of the OMIT phenomenon is the possibility of slow and fast light realization[27–35] which has important applications in quantum information and quantum communications. As is well-known in the standard OMIT phenomenon, the transmitted light intensity at the probe frequency in the cavity output is lower than or equal to that in the input where the equality (corresponding to 100% probe transmission) occurs when the damping rate of the mechanical oscillator is much lower than the optical damping rate. Nevertheless, there is a very interesting case in which the transmitted probe amplitude in the cavity output is stronger than that in the input of the cavity. In such a situation, the system exhibits a special kind of OMIT known as optomechanically induced gain (OMIG) or optomechanically induced amplification, so that it can be used as an optical transistor[36–44]. More recently, it has been shown[45,46] that the phenomenon of OMIG can occur in a bare OMS in the unresolved sideband (URSB) regime[47] while the coupling laser frequency has been tuned on the red sideband of the cavity (the red detuned regime of optomechanics). Although OMIG can be also achieved in the blue detuned regime of optomechanics, but the important problem is that OMSs are rarely stable in the blue regime.

Motivated by the above-mentioned investigations, in the present work we study a hybrid OMS consisting of an interacting BEC whose cavity is pumped by a coupling laser responsible for generation of an optical lattice inside the cavity. The optical lattice provides an effective optomechanical coupling between the cavity optical mode and the Bogoliubov mode of the BEC through a radiation pressure interaction. It is also assumed that the

[1]Laser and Plasma Research Institute, Shahid Beheshti University, Tehran, Iran. [2]Department of Physics, Shahid Beheshti University, Tehran, Iran. ✉email: a_dalafi@sbu.ac.ir

cavity is exposed to an input optical signal which is modeled as a time-dependent perturbation (playing the role of a weak probe laser).

Our aim in the present work is to demonstrate that the present hybrid OMS can be used as an optical transistor which can amplify the input optical signal in the output of the cavity. It is explicitly shown that in the URSB and red detuned regimes of optomechanics, the present hybrid OMS exhibits much larger gain in comparison to the previously studied schemes[36–44] while the system is stable. Furthermore, one of the most important advantages of the present scheme in comparison to the previous ones is the controllability of the system gain which can be manipulated not only through the coupling laser pumping rate but also through the *s*-wave scattering frequency of atomic collisions, which itself is experimentally controllable through the transverse trapping frequency of the BEC[48].

The structure of the paper is as follows: In section "System Hamiltonian" the Hamiltonian of the hybrid OMS is introduced. In section "Dynamics of the system" the dynamical equations of the system are derived based on the Heisenberg-Langevin equations and the response of the system to the input signal, which behaves as a time-dependent probe perturbation, is obtained. Then, in section "Results and discussion" we present the behavior of the system response to the input signal and the cavity power reflection coefficient. Finally, the summary and conclusions are given in section "Summary and conclusions".

System Hamiltonian

The studied system is a Fabry-Perot cavity with a length of L and a resonance frequency of ω_0 containing a trapped one dimensional BEC as has been shown in Fig. 1. The BEC has been formed by N identical two-level atoms having transition frequency ω_a and mass m_a confined in a cylindrically symmetric trap with a transverse trapping frequency $\omega_\perp$ and negligible longitudinal confinement along the x direction. The cavity is driven by a strong external (coupling) laser with a power of P_c and frequency ω_c at the rate of $|\varepsilon_c| = \sqrt{2\kappa_e P_c/\hbar\omega_c}$ along its axis from the partially transparent mirror on the left side of the cavity which is responsible to produce a radiation pressure coupling with the matter field of the BEC. In order to see how the present system acts as an optical transistor, it is assumed that a weak optical signal (playing the role of a probe laser) with frequency ω_s enters the cavity as an input coherent field through the left mirror at the rate of ε_s.

In the dispersive regime, where the difference between the frequency of the coupling laser and that of the atomic transition is much larger than the atomic linewidth (Γ_a), i.e., $\Delta_a = \omega_c - \omega_a \gg \Gamma_a$, the excited electronic state of the atoms can be adiabatically eliminated and spontaneous emission can be ignored[49,50], so that the second quantized Hamiltonian of the system can be written as

$$\begin{aligned}\hat{H} =& \hbar\omega_0\hat{a}^\dagger\hat{a} + \int_{-L/2}^{L/2} dx\hat{\Psi}^\dagger(x)\left(\frac{-\hbar^2}{2m_a}\frac{d^2}{dx^2} + \hbar U_0\cos^2(kx)\hat{a}^\dagger\hat{a} + \frac{1}{2}U_s\hat{\Psi}^\dagger(x)\hat{\Psi}(x)\right)\hat{\Psi}(x)\\ &+ i\hbar\left(\varepsilon_c e^{-i\omega_c t}\hat{a}^\dagger - \varepsilon_c^* e^{i\omega_c t}\hat{a}\right) + i\hbar\left(\varepsilon_s e^{-i\omega_s t}\hat{a}^\dagger - \varepsilon_s^* e^{i\omega_s t}\hat{a}\right),\end{aligned} \tag{1}$$

where $\hat{\Psi}(x)$ represents the atomic field annihilation operator in position space and $\hat{a}$ indicates the cavity mode annihilation operator in momentum space. Besides, $k = \omega_c/c$ is the wave number of the intracavity optical field, $U_0 = g_0^2/\Delta_a$ is the depth of the optical lattice potential per single-photon, g_0 is the vacuum Rabi frequency, $U_s = 4\pi\hbar^2 a_s/m_a$ is the strength of the atom-atom scattering wherein a_s is the length of the two-body s-wave scattering.

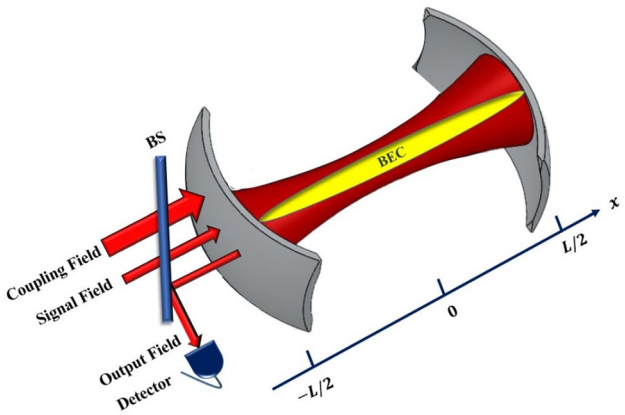

Figure 1. (Color online) A Fabry-Perot cavity containing a trapped BEC is driven by a strong coupling laser along its axis from the left mirror of the cavity where a weak input signal is also entered. The system behaves as an optical transistor that can amplify the input signal in the output which emanates from the left side of the cavity.

If the condition of $U_0\langle a^\dagger a\rangle \leq 10\omega_R$ is satisfied, in which $\omega_R = \hbar k^2/2m_a$ is the atom recoil frequency, the system is in weak optical lattice regime. Under this condition and using the Bogoliubov approximation, the matter field $\hat{\Psi}(x)$ can be expanded as[51]

$$\hat{\Psi}(x) = \sqrt{\frac{N}{L}} + \sqrt{\frac{2}{L}}\cos(2kx)\hat{c}, \tag{2}$$

where $\hat{c}$ is the BEC's first excited mode annihilation operator in the momentum space satisfying the commutation relation $[\hat{c}, \hat{c}^\dagger] = 1$.

By substituting Eq. (2) into Eq. (1), the system's Hamiltonian in the frame rotating at the coupling laser frequency can be rewritten as

$$\hat{H} = \hbar\delta_c\hat{a}^\dagger\hat{a} + \hbar\zeta\,\hat{a}^\dagger\hat{a}\hat{Q} + \frac{1}{2}\hbar\Omega_c\left(\hat{P}^2 + \hat{Q}^2\right) + \frac{1}{2}\hbar\omega_{sw}\hat{Q}^2 + i\hbar\left(\varepsilon_c\hat{a}^\dagger - \varepsilon_c^*\hat{a}\right) + i\hbar\left(\varepsilon_s e^{-i\delta t}\hat{a}^\dagger - \varepsilon_s^* e^{i\delta t}\hat{a}\right), \tag{3}$$

where $\delta = \omega_s - \omega_c$ is the detuning between the frequencies of the coupling and signal lasers. Besides, $\hat{Q} = (\hat{c} + \hat{c}^\dagger)/\sqrt{2}$ and $\hat{P} = (\hat{c} - \hat{c}^\dagger)/\sqrt{2}i$ are, respectively, the position and momentum quadratures of the BEC satisfying the commutation relation $[\hat{Q}, \hat{P}] = i$. Furthermore, $\delta_c = \Delta_c + \frac{1}{2}NU_0$ is the Stark-shifed cavity frequency due to the presence of the BEC in which $\Delta_c = \omega_0 - \omega_c$ is the cavity resonance detuning with the frequency of the coupling laser. In fact, the presence of the BEC makes the bare resonance frequency of the cavity be changed from ω_0 to $\omega_0 + \frac{1}{2}NU_0$. As is seen from the second and third terms of Eq. (3), the BEC behaves as a mechanical oscillator (the so-called Bogoliubov mode) with the frequency $\Omega_c = 4\omega_R + \omega_{sw}/2$ that has been coupled to the optical mode of the cavity through the optomechanical coupling parameter of $\zeta = \frac{1}{2}\sqrt{N}U_0$. Besides, the effect of atom-atom interaction with the s-wave scattering frequency $\omega_{sw} = 8\pi\hbar a_s N/m_a L w^2$ leads to the manifestation of the fourth term in Eq. (3), where w is the waist radius of the optical mode.

Dynamics of the system

In this section, we study the dynamics of the system with the Hamiltonian of Eq. (3) in the framework of open quantum systems which is described by the following Heisenberg-Langevin equations of motion

$$\frac{d\hat{a}}{dt} = -(\kappa + i\delta_c)\hat{a} - \zeta\hat{Q}\hat{a} + \varepsilon_c + \varepsilon_s e^{-i\delta t} + \sqrt{2\kappa_e}\hat{a}_{in} + \sqrt{2\kappa_i}\hat{a}_{int}, \tag{4a}$$

$$\frac{d\hat{P}}{dt} = -\gamma_B\hat{P} - (\Omega_c + \omega_{sw})\hat{Q} - \zeta\hat{a}^\dagger\hat{a} + \hat{P}_{in}, \tag{4b}$$

$$\frac{d\hat{Q}}{dt} = \Omega_c\hat{P}, \tag{4c}$$

where $\sqrt{2\kappa_e}\hat{a}_{in}$ and $\sqrt{2\kappa_i}\hat{a}_{int}$ are the input and internal noises, which are respectively originated by the input-output coupling and non-perfectness of the mirrors or light scattering of the remaining air molecules inside the cavity (κ_i is the cavity internal decay rate). In principle, the dissipation of the intracavity field takes place in two different ways: the first one is the leakage that occurs through the left mirror with the rate of κ_e which appears as the output field of the cavity that is detected on the left mirror, and the second one is the loss that occurs through inaccessible channels with the rate of κ_i. Therefore the cavity field amplitude damping rate is $\kappa = \kappa_e + \kappa_i$[52]. Furthermore, the output coupling ratio is defined by the coupling parameter ($r_c = \kappa_e/\kappa$) and the damping rate of the Bogoliubov mode of the BEC is denoted by γ_B. Here $\hat{P}_{in}$ is the BEC atomic field input noise, whose mean value is zero.

Assuming no correlation between any two system operators, i.e., $\langle\hat{a}\hat{b}\rangle = \langle\hat{a}\rangle\langle\hat{b}\rangle$, which is called the mean-field approximation, and supposing that $\langle\hat{a}_{in}\rangle = \langle\hat{a}_{int}\rangle = \langle\hat{P}_{in}\rangle = 0$, the mean-value equations of motion for $\hat{a}$, $\hat{P}$, and $\hat{Q}$ from Eqs. (4a–4c) can be obtained as

$$\frac{d\langle\hat{a}\rangle}{dt} = -(\kappa + i\delta_c)\langle\hat{a}\rangle - \zeta\langle\hat{Q}\rangle\langle\hat{a}\rangle + \varepsilon_c + \varepsilon_s e^{-i\delta t}, \tag{5a}$$

$$\frac{d\langle\hat{P}\rangle}{dt} = -\gamma_B\langle\hat{P}\rangle - (\Omega_c + \omega_{sw})\langle\hat{Q}\rangle - \zeta\langle\hat{a}^\dagger\rangle\langle\hat{a}\rangle, \tag{5b}$$

$$\frac{d\langle\hat{Q}\rangle}{dt} = \Omega_c\langle\hat{P}\rangle. \tag{5c}$$

By eliminating $\langle\hat{P}\rangle$ from Eqs. (5b) and (5c) the dynamical equation of motion for the mean-value of $\hat{Q}$ operator of the BEC Bogoliubov mode is obtained as the following second order differential equation

$$\frac{d^2\langle\hat{Q}\rangle}{dt^2} + \gamma_B\frac{d\langle\hat{Q}\rangle}{dt} + \omega_B^2\langle\hat{Q}\rangle = -\Omega_c\zeta\langle\hat{a}^\dagger\rangle\langle\hat{a}\rangle. \tag{6}$$

As is seen from Eq. (6) the Bogoliubov mode of the BEC behaves as a driven-damped simple harmonic oscillator with an effective resonance frequency of $\omega_B = \sqrt{(4\omega_R + \frac{1}{2}\omega_{sw})(4\omega_R + \frac{3}{2}\omega_{sw})}$, which is called the Bogoliubov frequency.

In the case where the signal field amplitude is much smaller than the coupling field amplitude, i.e., $|\varepsilon_s| \ll |\varepsilon_c|$, the steady state solutions to Eqs. (5a) and (6), to the first order of $|\varepsilon_s|$ in the frame rotating at ω_c can be written as

$$\langle \hat{a} \rangle = a_0 + a_+ e^{-i\delta t} + a_- e^{i\delta t}, \tag{7a}$$

$$\langle \hat{Q} \rangle = Q_0 + Q_+ e^{-i\delta t} + Q_- e^{i\delta t}. \tag{7b}$$

The right hand side of Eqs. (7a) and (7b) contain three terms corresponding to the first three components of the Fourier expansion which are the steady state solutions at zero, first, and second order of ε_s, respectively oscillating at the coupling laser frequency ω_c, signal field frequency ω_s, and the four-wave mixing frequency $2\omega_c - \omega_s$ in the laboratory frame[36]. Now, by inserting Eqs. (7a) and (7b) in Eqs. (5a) and (6), the zeroth order components can be derived as

$$a_0 = \frac{\varepsilon_c}{\kappa + i\Delta}, \tag{8a}$$

$$Q_0 = \frac{-\Omega_c \zeta |a_0|^2}{\omega_B^2}, \tag{8b}$$

wherein $\Delta = \delta_c + \zeta Q_0$ is the effective cavity detuning. Furthermore, by equalizing the coefficients with the same frequencies on both sides of the equations of motion, the following algebraic equations can be obtained

$$\big(i(\Delta - \delta) + \kappa\big) a_+ = -i\zeta a_0 Q_+ + \varepsilon_s, \tag{9a}$$

$$\big(i(\Delta + \delta) + \kappa\big) a_- = -i\zeta a_0 Q_-, \tag{9b}$$

$$\big(\omega_B^2 - \delta^2 + i\gamma_B \delta\big) Q_+ = -\Omega_c \zeta \big(a_0^* a_+ + a_0 a_-^*\big), \tag{9c}$$

$$\big(\omega_B^2 - \delta^2 - i\gamma_B \delta\big) Q_- = -\Omega_c \zeta \big(a_0 a_+^* + a_0^* a_-\big). \tag{9d}$$

Assuming a_0 is real, the solutions of Eqs. (9a–9d) are obtained as follows

$$a_+ = \frac{1 + if}{i(\Delta - \delta) + \kappa - 2f\Delta} \varepsilon_s, \tag{10a}$$

$$a_- = -\frac{a_+^*}{1 + i/f^*}, \tag{10b}$$

$$Q_- = Q_+^*, \tag{10c}$$

wherein $\chi = \frac{\Omega_c}{\omega_B^2 - \delta^2 - i\gamma_B \delta}$ is called the mechanical susceptibility of the BEC Bogoliubov mode and f is defined as $f = \frac{\chi \zeta^2 a_0^2}{-i(\Delta+\delta)+\kappa}$.

Since we are going to derive the amplitude of the cavity output field emanating through the left mirror, we make use of the input-output relation, $\varepsilon_{out} + \varepsilon_{in} = 2\kappa_e \langle \hat{a} \rangle$, where ε_{in} and ε_{out} are, respectively, the cavity input and output field amplitudes. Similar to relations (7a) and (7b), the cavity output field amplitude in the rotating frame can be written as follows

$$\varepsilon_{out} = \varepsilon_{out0} + \varepsilon_{out+} e^{-i\delta t} + \varepsilon_{out-} e^{i\delta t}, \tag{11}$$

where ε_{out0} is the central band amplitude of the cavity output field oscillating at the frequency ω_c while ε_{out+} and ε_{out-} are the two sidebands oscillating, respectively, at frequencies ω_s and $2\omega_c - \omega_s$ in the laboratory frame. Based on Eq. (4a), the input field amplitude is $\varepsilon_{in} = \varepsilon_c + \varepsilon_s e^{-i\delta t}$. If we substitute the input field amplitude as well as $\langle \hat{a} \rangle$ and ε_{out} from Eqs. (7a) and (11) in the input-output relation, the central band amplitude of the output field is obtained as $\varepsilon_{out0} = 2\kappa_e a_0 - \varepsilon_c$, while the two sideband amplitudes are determined by $\varepsilon_{out+} = 2\kappa_e a_+ - \varepsilon_s$, and $\varepsilon_{out-} = 2\kappa_e a_-$.

The cavity reflected field amplitude oscillating at the signal frequency is defined as the ratio of the cavity reflected field amplitude oscillating at the signal frequency (ε_{out+}) to the input signal field amplitude (ε_s), i.e., $\varepsilon_R = \varepsilon_{out+}/\varepsilon_s$. In the critical regime, where the rate of the cavity inaccessible loss (κ_i) is equal to the loss rate of the intracavity optical field (κ_e), the coupling parameter is $r_c = 1/2$, and the cavity reflected field amplitude at the signal frequency is obtained as

$$\varepsilon_R = \frac{\kappa(1+if)}{i(\Delta-\delta)+\kappa-2f\Delta} - 1. \tag{12}$$

Finally, the cavity power reflection coefficient at the signal frequency is defined as the square of the reflected field amplitude at the signal frequency as

$$R = |\varepsilon_R|^2. \tag{13}$$

Results and discussion

In order to investigate how the present hybrid OMS behaves as an optical transistor that can amplify the input signal, we study the behavior of the real part of reflected field amplitude given by Eq. (12), which represents the cavity absorptive behavior at the signal frequency, as well as the cavity power reflection coefficient at the signal frequency (Eq. (13)) in terms of the coupling-signal detuning $\delta = \omega_s - \omega_c$ in the regime where the system is stable.

Here, our results have been obtained based on the experimentally feasible parameters given in Refs.[53,54]. We have considered a cavity with the length of $L = 178\,\mu$m, damping rate of $\kappa = 10^6$ Hz, and bare frequency of $\omega_0 = 2.41494 \times 10^{15}$ Hz which corresponds to a wavelength of $\lambda = 780$ nm. The cavity contains a trapped BEC formed by $N = 10^6$ Rb atoms having a transition frequency of $\omega_a = 2.41419 \times 10^{15}$ Hz. The strength of the atom-field coupling is $g_0 = 2\pi \times 14.1$ MHz, the atom recoil frequency is $\omega_R = 23.7$ kHz, and the BEC damping rate of the Bogoliubov mode of the BEC is $\gamma_B = 10^{-4}\kappa$.

In order that the system is on-resonance, we obtain our results in the red detuning regime of $\Delta = \omega_B$ which leads to the following cubic equation in terms of ω_c

$$\omega_0 - \omega_c + \frac{1}{2}\frac{Ng_0^2}{\omega_c - \omega_a} - \frac{Ng_0^4\Omega_c}{4\omega_B^2}\frac{|a_0|^2}{(\omega_c-\omega_a)^2} = \omega_B. \tag{14}$$

For any specified value of ω_{sw} the value of ω_B and subsequently the square of the optical zero-order component, i.e, $|a_0|^2 = |\varepsilon_c|^2/(\kappa^2+\omega_B^2)$ are determined based on Eq. (8a). Since Eq. (14) is a third order algebraic equation, it has three roots for each value of ω_{sw}. However, only for one of them the system is stable according to the Routh-Hurwitz criteria[55].

In Fig. 2, the stable and unstable regions of the system have been indicated based on the Routh-Hurwitz criteria as a contour plot in terms of two experimentally controllable parameters of the system: the normalized coupling laser pumping rate ($|\varepsilon_c|/\kappa$) and the normalized s-wave scattering frequency (ω_{sw}/ω_R). The stable and unstable regions have been shown, respectively, by blue and red colors. Experimentally, the coupling laser pumping rate can be controlled by the power of the coupling laser while the *s*-wave scattering frequency of atomic collisions can be manipulated by the transverse frequency of the optical trap of the BEC?. Figure 2 shows that for $|\varepsilon_c| \geq 0.14\kappa$ the *s*-wave scattering frequency is bound to have a nonzero minimum value so that the system remains in the stable regime, where the mentioned minimum of ω_{sw} increases by increasing $|\varepsilon_c|$. On the other

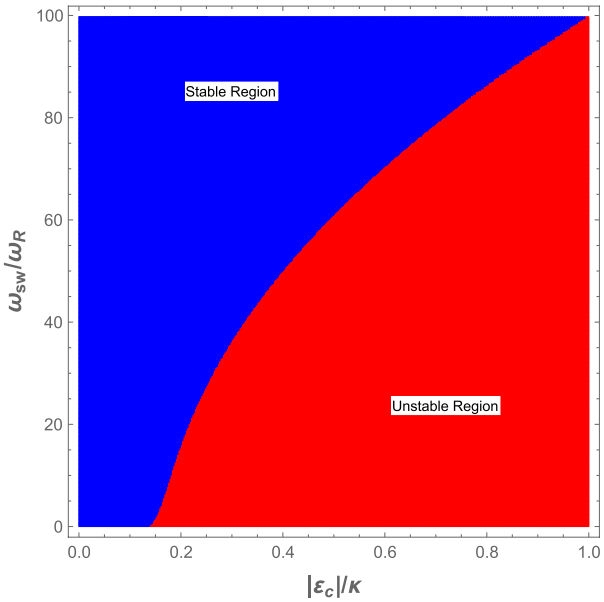

Figure 2. (Color online) The stable (blue) and unstable (red) regions, derived from the Routh-Hurwitz criteria where the horizontal axis is the normalized coupling laser pumping rate ($|\varepsilon_c|/\kappa$) and the vertical axis is the normalized s-wave scattering frequency (ω_{sw}/ω_R). The parameters are given in the second paragraph of section "Results and discussion".

hand, for any fixed value of the s-wave scattering frequency, $|\varepsilon_c|$ should be lower than a maximum value so that the system is stable.

To study the mechanism of the system response to the input signal, we have plotted in Fig. 3 the real and imaginary parts of the output (reflected) field amplitude as well as the cavity power reflection coefficient at the input signal frequency versus the normalized frequency detuning (δ/κ) when the system is in the red detuning regime of $\Delta = \omega_B$. Here the coupling laser pumping rate has been fixed at $|\varepsilon_c| = 0.10\kappa$ for two different values of the s-wave scattering frequency of atomic collisions: $\omega_{sw} = 100\omega_R$ (Fig. 3a), and $\omega_{sw} = 30\omega_R$ (Fig. 3b). For each value of ω_{sw} the effective frequency of the Bogoliubov mode of the BEC, which plays the role of the mechanical mode frequency in the present hybrid OMS, is determined to be $\omega_B \approx 2.16\kappa$ in Fig. 3a and $\omega_B \approx 0.72\kappa$ in Fig. 3b. For each mentioned value of ω_B one can solve Eq. (14) to find three roots for ω_c which just one of them is acceptable based on the stability condition of the Routh-Hurwitz criteria. In this way, in an experimental setup with specified values of ε_c and ω_{sw}, the right value of the coupling laser frequency (ω_c) can be determined so that if the cavity is driven at that frequency, the system response to the input signal appears as those demonstrated in Fig. 3a and 3b. Here, the three roots of Eq. (14) are approximately given by 2.41494×10^{15}, 2.41419×10^{15}, and 2.41418×10^{15}, where the first root satisfies the stability conditions. In this way, the right value of the coupling laser frequency is $\omega_c \approx 2.41494 \times 10^{15}$Hz.

In the present system, the input signal acts as a time-dependent perturbation (the last term in the Hamiltonian of Eq. (3)) where the absorptive and dispersive responses of the system to it are manifested, respectively, in the real and imaginary parts of the output (reflected) field amplitude. Since in Fig. 3a and b the enhanced effective optomechanical coupling $\zeta a_0 < \kappa/2$ the system is in the OMIT regime[56] where a fairly narrow transparency window appears at $\delta = \omega_B$. That is why the dip of the transparency window of the OMIT in Fig. 3a and 3b occurs, respectively at $\delta \approx 2.16\kappa$ and $\delta \approx 0.72\kappa$. Besides, since at the center of the transparency window $Im[\varepsilon_R] = 0$ and $Re[\varepsilon_R] \leq -1$, the power reflection coefficient is determined by $R = |Re[\varepsilon_R]|^2$, which is in the range of $R \geq 1$. When the maximum value of the power reflection coefficient at the signal frequency is greater than one, the phenomenon of OMIG[45] happens and the cavity acts as an amplifier[57].

Since ω_B is an increasing function of ω_{sw}, for large values of ω_{sw}, like the case of Fig. 3a, the system is in the resolved sideband (RSB) regime, where $\omega_B > \kappa$, while for small values of ω_{sw}, like the case of Fig. 3b, the system is in the URSB regime, where $\omega_B < \kappa$. In this way, the position of the dip of absorptive response (the red curves) indicates whether the system is in RSB or URSB regimes. Therefore, the system regime can be switched from RSB to URSB or vice versa by manipulating ω_{sw} which itself is controllable through the transverse trapping frequency of the BEC[48]. As is seen from Fig. 3a, where the system is in the RSB regime, $Re[\varepsilon_R] \approx -1$ and consequently $R \approx 1$ which corresponds to the situation of the standard OMIT where the reflection of the input signal is nearly 100%. However, in the URSB regime $Re[\varepsilon_R] < -1$ and consequently, $R > 1$ which corresponds to the OMIG in which the input signal is amplified in the output of the system. As is seen from Fig. 3b the input signal power can be increased more than two times in the output of the cavity since $Re[\varepsilon_R] < -2$ and consequently $R > 2$.

In Fig. 4, we have plotted the real part of the reflected field amplitude of the system (Fig. 4a) and the cavity power reflection coefficient (Fig. 4b) at the signal frequency versus the normalized coupling-signal detuning (δ/κ) for $|\varepsilon_c| = 0.10\kappa$ and three different values of the s-wave scattering frequency: $\omega_{sw} = 5\omega_R, 10\omega_R$, and $15\omega_R$ represented, respectively, by red thick, black dashed and blue thin curves. It should be emphasized that for $|\varepsilon_c| = 0.10\kappa$ the values of ω_{sw} have been so considered that the system is in the stable (blue) region of Fig. 2. Each curve in Fig. 4a, which is a dip of the OMIT transparency window like that of the absorptive response (red thick curve) in Fig. 3, corresponds to a specified value of ω_{sw} for which the cavity is driven at the specified value of ω_c determined based on Eq. (14). Figure 4b shows that there exists a peak of power reflection coefficient corresponding to each dip in Fig. 4a. Since all the dips of the OMIT transparency windows in Fig. 4a occur at $\delta = \omega_B < \kappa$, the system is in the URSB regime in which it acts as an amplifier. As is seen, the deeper is the dip

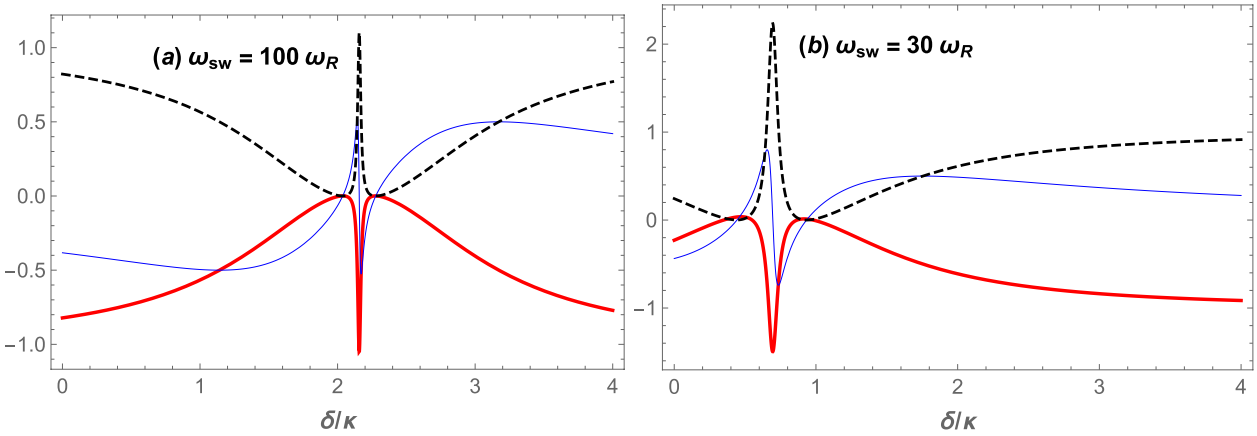

Figure 3. (Color online) $Re[\varepsilon_R]$ (red thick curve) and $Im[\varepsilon_R]$ (blue thin curve) as well as the cavity power reflection coefficient R (black dashed curve) at the signal frequency versus the normalized frequency detuning (δ/κ) for the coupling laser pumping rate of $|\varepsilon_c| = 0.10\kappa$, in the red detuning regime of $\Delta = \omega_B$ for two different values of the s-wave scattering frequency: (**a**) $\omega_{sw} = 100\omega_R$, and (**b**) $\omega_{sw} = 30\omega_R$. The other parameters are the same as those of Fig. 2.

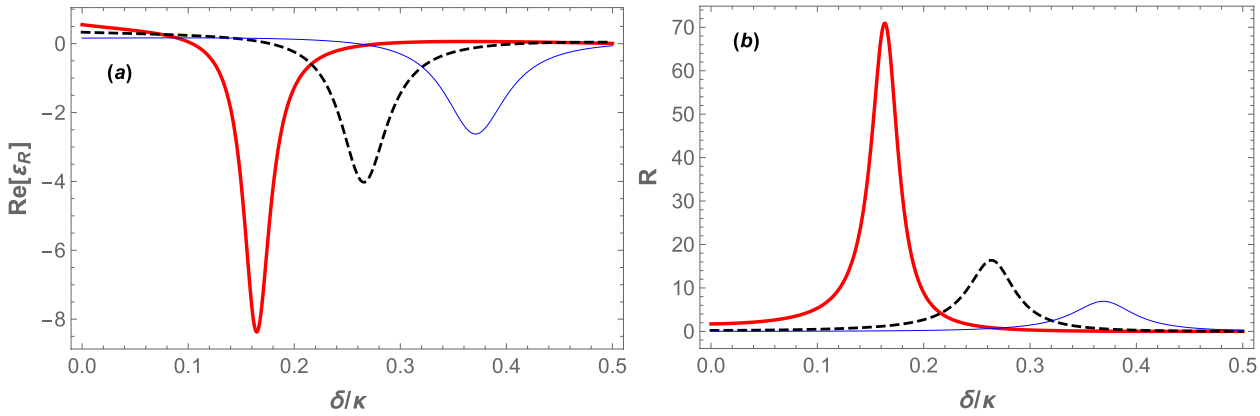

Figure 4. (Color online) (**a**) The real part of the reflected field amplitude. (**b**) The cavity power reflection coefficient at the signal frequency, versus the normalized frequency detuning (δ/κ), for the coupling laser pumping rate at $|\varepsilon_c| = 0.10\kappa$ and three different values of ω_{sw}, in the red detuning regime where $\Delta = \omega_B$. The red thick, black dashed, and blue thin plots correspond to the values of $\omega_{sw} = 5\omega_R$, $\omega_{sw} = 10\omega_R$ and $\omega_{sw} = 15\omega_R$, respectively. The other parameters are the same as those of Fig. 2.

of the transparency window, the larger is the peak of the power reflection coefficient of the system (the more amplification) so that for $\omega_{sw} = 5\omega_R$ the amplitude of the input signal is amplified up to 70 times in the output of the cavity, i.e., 7000% amplification.

To see how the amplification capacity of the system can be enhanced, in Fig. 5a we have plotted the minimum of the real part of the reflected field amplitude (corresponding to the minimum values of OMIT dips of Fig. 4a which occur at $\delta = \omega_B$ for every ω_{sw}), and also we have plotted in Fig. 5b the maximum values of the power reflection coefficient at the signal frequency (corresponding to the maximum values of peaks of Fig. 4b) versus ω_{sw}/ω_R for two different values of coupling laser pumping rate: $|\varepsilon_c| = 0.10\kappa$ (the blue thin curves), and $|\varepsilon_c| = 0.15\kappa$ (the red thick curves). It should be noted that the variation range of ω_{sw} in Fig. 5 has been chosen so that the system is stable and in the URSB regime. According to Fig. 5a, by decreasing ω_{sw} the negativity of the real part of the reflected field amplitude increases, and consequently the maximum power reflection coefficient (amplification capacity) increases for each value of $|\varepsilon_c|$. Furthermore, as is seen from Fig. 5b at any ω_{sw} the maximum value of the power reflection coefficient has a larger value for a larger $|\varepsilon_c|$ (compare the red thick and blue thin curves). For example, at $\omega_{sw} = 3\omega_R$ the maximum value of the power reflection coefficient is more than 2000 (corresponding to 2×10^5% amplification) for $|\varepsilon_c| = 0.15\kappa$, while it is about 200 (corresponding to 2×10^4% amplification) for $|\varepsilon_c| = 0.10\kappa$.

Furthermore, to show explicitly how the maximum value of the power reflection coefficient at the signal frequency increases by increasing the coupling laser pumping rate, in Fig. 6, we have plotted $Max[R]$ versus the normalized coupling laser pumping rate ($|\varepsilon_c|/\kappa$), for three different values of the s-wave scattering frequency: $\omega_{sw} = 3\omega_R$ (red thick curve), $\omega_{sw} = 4\omega_R$ (black dashed curve), and $\omega_{sw} = 5\omega_R$ (the blue thin curve). The inset of Fig. 6 shows $Max[R]$ versus $|\varepsilon_c|/\kappa$ for $\omega_{sw} = \omega_R$. As is seen from Fig. 6, $Max[R]$ increases very rapidly by increasing the coupling laser pumping rate where the system gets near to the boundary of the instability region

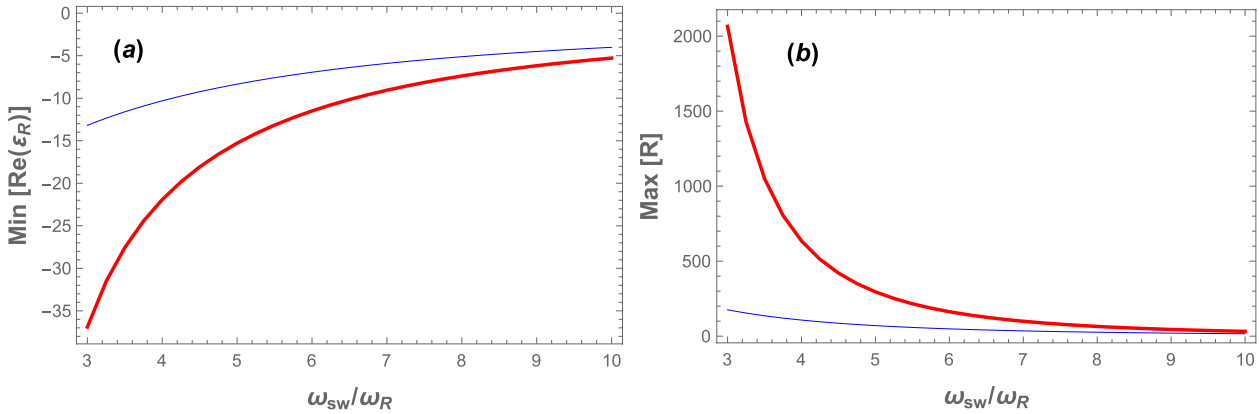

Figure 5. (Color online) (**a**) The minimum value of the real part of the reflected field amplitude, (**b**) the maximum value of the cavity power reflection coefficient at the signal frequency versus ω_{sw}/ω_R for two different values of the coupling laser pumping rate: $|\varepsilon_c| = 0.10\kappa$ (the blue thin curve) and $|\varepsilon_c| = 0.15\kappa$ (the red thick curve). The other parameters are the same as those of Fig. 2.

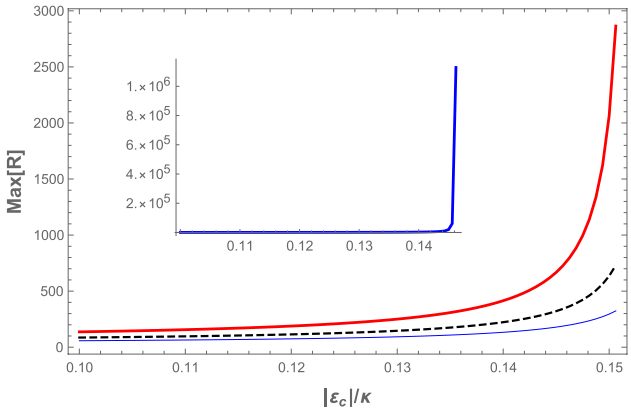

Figure 6. (Color online) The maximum value of the cavity power reflection coefficient at the signal frequency versus the normalized coupling laser pumping rate ($|\varepsilon_c|/\kappa$) for different values of the *s*-wave scattering frequency: $\omega_{sw} = 3\omega_R$ (red thick curve), $\omega_{sw} = 4\omega_R$ (black dashed curve) and $\omega_{sw} = 5\omega_R$ (blue thin curve). The inset shows $Max[R]$ versus $|\varepsilon_c|/\kappa$ for $\omega_{sw} = \omega_R$. The other parameters are the same as those of Fig. 2.

for each ω_{sw} (the red region in Fig. 2). Besides, this increase is more intense for lower values of ω_{sw} so that for $\omega_{sw} = \omega_R$ (the inset of Fig. 6) the maximum value of the power reflection coefficient at the signal frequency exceeds 10^6 before the system enters the instability regime. It means that in the red detuned and URSB regime, the present hybrid OMS can amplify the input signal more than 10^8% while it is in the stable regime. This result is much greater than those obtained in the previously proposed schemes[36–41,45], and specifically three orders of magnitude larger than that obtained in Ref.[39], where it has been shown that in the hybrid OMS (in which the effect of atom-atom interaction is neglected and no stability check has been presented) the maximum amplification that can be achieved is less than 2×10^5% in the blue regime of optomechanics, where the system has usually stability problems.

Finally, it is worth reminding that another scheme for the generation of gain in OMSs has been already proposed based on the coherent modulation of the mechanical oscillator[58]. Such a scheme can lead to the generation of Casimir photons and phonons[59] which makes the system act as a quantum amplifier or squeezer[60] or behave as a quantum sensor for weak force sensing below the standard quantum limit (SQL)[61–63]. As an interesting outlook for future researches, one can investigate the possibility of manifestation of OMIG in bare or hybrid OMSs whose mechanical modes are coherently modulated in the URSB regime. One of the best methods for studying the response of such driven-dissipative systems is the approach of Green's function and the linear response theory[64–68]which have been recently attracted much attention.

Summary and conclusions

We have studied the phenomenon of OMIG in a hybrid OMS consisting of a one dimensional BEC whose cavity is driven by a coupling laser tuned to the red sideband of the cavity in order to generate an effective optomechanical coupling between the optical mode of the cavity and the Bogoliubov mode of the BEC. It has been shown that if the cavity is exposed to a weak input signal behaving as an external signal laser which drives the intracavity mode perturbatively, the system acts as an optical transistor that can magnify the input signal in its output while the system is in the URSB regime. For this purpose, we have solved the Heisenberg-Langevin equations to obtain the reflected field amplitude in the cavity output whose real and imaginary parts represent, respectively, the absorptive and dispersive response of the system to the input signal. We have also shown that the system can switch from RSB to URSB by manipulating the *s*-wave scattering frequency which itself can be controlled by the transverse trapping frequency of the BEC. More importantly, we have shown that the amount of the system amplification can be enhanced and controlled by the coupling laser power as well as the *s*-wave scattering frequency as far as the system is stable and in the URSB regime. It has been shown that by decreasing the *s*-wave scattering frequency from one hand, and by increasing the coupling laser power from the other hand, the cavity power reflection coefficient at the signal frequency can be enhanced considerably before the system enters the instability region. Based on our obtained results, the input signal can be amplified more than 10^8% which is much larger than those obtained in previous studies.

Data availibility

All data that support the findings of this study are included within the article.

Received: 10 December 2022; Accepted: 27 February 2023
Published online: 04 March 2023

References

1. Maschler, C., Mekhov, I. B. & Ritsch, H. Ultracold atoms in optical lattices generated by quantized light fields. *Eur. Phys. J. D* **46**, 545–560 (2008).
2. Kanamoto, R. & Meystre, P. Optomechanics of ultracold atomic gases. *Phys. Scr.* **82**, 038111 (2010).

3. Asjad, M. Cavity optomechanics with a bose-einstein condensate: Normal mode splitting. *J. Mod. Opt.* **59**, 917–922 (2012).
4. Chen, B., Jiang, C. & Zhu, K.-D. Tunable all-optical kerr switch based on a cavity optomechanical system with a bose-einstein condensate. *JOSA B* **28**, 2007–2013 (2011).
5. Asjad, M. Electromagnetically-induced transparency in optomechanical systems with bose-einstein condensate. *J. Russ. Laser Res.* **34**, 159–165 (2013).
6. Aspelmeyer, M., Kippenberg, T. J. & Marquardt, F. Cavity optomechanics. *Rev. Mod. Phys.* **86**, 1391 (2014).
7. Brennecke, F. *et al.* Cavity qed with a bose–einstein condensate. *nature* **450**, 268–271 (2007).
8. Gupta, S., Moore, K. L., Murch, K. W. & Stamper-Kurn, D. M. Cavity nonlinear optics at low photon numbers from collective atomic motion. *Phys. Rev. Lett.* **99**, 213601 (2007).
9. Domokos, P. & Ritsch, H. Mechanical effects of light in optical resonators. *JOSA B* **20**, 1098–1130 (2003).
10. Maschler, C. & Ritsch, H. Cold atom dynamics in a quantum optical lattice potential. *Phys. Rev. Lett.* **95**, 260401 (2005).
11. Kónya, G., Szirmai, G. & Domokos, P. Multimode mean-field model for the quantum phase transition of a bose-einstein condensate in an optical resonator. *Eur. Phys. J. D* **65**, 33–42 (2011).
12. Dalafi, A., Naderi, M., Soltanolkotabi, M. & Barzanjeh, S. Nonlinear effects of atomic collisions on the optomechanical properties of a bose-einstein condensate in an optical cavity. *Phys. Rev. A* **87**, 013417 (2013).
13. Asjad, M. & Saif, F. Normal mode splitting in hybrid bec-optomechanical system. *Optik* **125**, 5455–5460 (2014).
14. Agarwal, G. S. & Huang, S. Electromagnetically induced transparency in mechanical effects of light. *Phys. Rev. A* **81**, 041803 (2010).
15. Huang, S. & Agarwal, G. Electromagnetically induced transparency from two-phonon processes in quadratically coupled membranes. *Phys. Rev. A* **83**, 023823 (2011).
16. Agarwal, G. & Huang, S. Optomechanical systems as single-photon routers. *Phys. Rev. A* **85**, 021801 (2012).
17. Weis, S. *et al.* Optomechanically induced transparency. *Science* **330**, 1520–1523 (2010).
18. Szirmai, G., Nagy, D. & Domokos, P. Quantum noise of a bose-einstein condensate in an optical cavity, correlations, and entanglement. *Phys. Rev. A* **81**, 043639 (2010).
19. Dalafi, A., Naderi, M. & Soltanolkotabi, M. Squeezed-state generation via atomic collisions in a bose-einstein condensate inside an optical cavity. *J. Mod. Opt.* **61**, 1387–1397 (2014).
20. Dalafi, A. & Naderi, M. Phase noise and squeezing spectra of the output field of an optical cavity containing an interacting bose-einstein condensate. *J. Phys. B: At. Mol. Opt. Phys.* **49**, 145501 (2016).
21. Dalafi, A. & Naderi, M. Dispersive interaction of a bose-einstein condensate with a movable mirror of an optomechanical cavity in the presence of laser phase noise. *Phys. Rev. A* **94**, 063636 (2016).
22. Dalafi, A., Naderi, M., Soltanolkotabi, M. & Barzanjeh, S. Controllability of optical bistability, cooling and entanglement in hybrid cavity optomechanical systems by nonlinear atom-atom interaction. *J. Phys. B: At. Mol. Opt. Phys.* **46**, 235502 (2013).
23. Dalafi, A. & Naderi, M. Controlling steady-state bipartite entanglement and quadrature squeezing in a membrane-in-the-middle optomechanical system with two bose-einstein condensates. *Phys. Rev. A* **96**, 033631 (2017).
24. Dalafi, A., Naderi, M. & Soltanolkotabi, M. The effect of atomic collisions on the quantum phase transition of a bose-einstein condensate inside an optical cavity. *J. Phys. B: At. Mol. Opt. Phys.* **48**, 115507 (2015).
25. Dalafi, A. & Naderi, M. Intrinsic cross-kerr nonlinearity in an optical cavity containing an interacting bose-einstein condensate. *Phys. Rev. A* **95**, 043601 (2017).
26. Dalafi, A., Naderi, M. & Motazedifard, A. Effects of quadratic coupling and squeezed vacuum injection in an optomechanical cavity assisted with a bose-einstein condensate. *Phys. Rev. A* **97**, 043619 (2018).
27. Tarhan, D., Huang, S. & Müstecaplıoğlu, Ö. E. Superluminal and ultraslow light propagation in optomechanical systems. *Phys. Rev. A* **87**, 013824 (2013).
28. Wu, Z. *et al.* Force-induced transparency and conversion between slow and fast light in optomechanics. *Phys. Rev. A* **96**, 033832 (2017).
29. Mikaeili, H., Dalafi, A., Ghanaatshoar, M. & Askari, B. Ultraslow light realization using an interacting bose-einstein condensate trapped in a shallow optical lattice. *Sci. Rep.* **12**, 1–10 (2022).
30. Han, C.-M., Wang, X., Chen, H. & Li, H.-R. Tunable slow and fast light in an atom-assisted optomechanical system with a mechanical pump. *Opt. Commun.* **456**, 124605 (2020).
31. Liao, Q., Xiao, X., Nie, W. & Zhou, N. Transparency and tunable slow-fast light in a hybrid cavity optomechanical system. *Opt. Express* **28**, 5288–5305 (2020).
32. Li, X.-X., Li, J.-Y., Cheng, X.-X. & Li, G.-A. Optical response with tunneling coupling in a hybrid optomechanical system. *Int. J. Theor. Phys.* **61**, 1–12 (2022).
33. Chen, B., Xing, H.-W., Chen, J.-B., Xue, H.-B. & Xing, L.-L. Tunable fast-slow light conversion based on optomechanically induced absorption in a hybrid atom-optomechanical system. *Quant. Inf. Process.* **20**, 1–11 (2021).
34. Chen, B., Jiang, C. & Zhu, K.-D. Slow light in a cavity optomechanical system with a bose-einstein condensate. *Phys. Rev. A* **83**, 055803 (2011).
35. Safavi-Naeini, A. H. *et al.* Electromagnetically induced transparency and slow light with optomechanics. *Nature* **472**, 69–73 (2011).
36. Huang, S. & Agarwal, G. Normal-mode splitting and antibunching in stokes and anti-stokes processes in cavity optomechanics: Radiation-pressure-induced four-wave-mixing cavity optomechanics. *Phys. Rev. A* **81**, 033830 (2010).
37. Li, J., Chu, Y., Liu, J. & Zhu, K.-D. Optomechanical transistor with phonons and photons. *IEEE Sens. J.* **17**, 3041–3044 (2017).
38. Wang, X.-Y., Si, L.-G., Liu, Z.-X., Lu, X.-H. & Wu, Y. Tunable optical amplification arising from blue detuning in a quadratically coupled optomechanical system. *JOSA B* **36**, 1355–1362 (2019).
39. Chen, B., Jiang, C., Li, J.-J. & Zhu, K.-D. All-optical transistor based on a cavity optomechanical system with a bose-einstein condensate. *Phys. Rev. A* **84**, 055802 (2011).
40. Si, L.-G., Xiong, H., Zubairy, M. S. & Wu, Y. Optomechanically induced opacity and amplification in a quadratically coupled optomechanical system. *Phys. Rev. A* **95**, 033803 (2017).
41. Zhang, X., Tian, L. & Li, Y. Optomechanical transistor with mechanical gain. *Phys. Rev. A* **97**, 043818 (2018).
42. Goodarzi, A., Ghanaatshoar, M. & Mozafari, M. All-optical fiber optic coherent amplifier. *Sci. Rep.* **8**, 1–6 (2018).
43. Goodarzi, A. & Ghanaatshoar, M. Controlling light by light: Photonic crystal-based coherent all-optical transistor. *JOSA B* **33**, 1594–1599 (2016).
44. Goodarzi, A. & Ghanaatshoar, M. Coherent all-optical transistor based on frustrated total internal reflection. *Sci. Rep.* **8**, 1–8 (2018).
45. Yan, X.-B. Optomechanically induced transparency and gain. *Phys. Rev. A* **101**, 043820 (2020).
46. Yan, X.-B. Optomechanically induced optical responses with non-rotating wave approximation. *J. Phys. B: At. Mol. Opt. Phys.* **54**, 035401 (2021).
47. Bennett, J. Quantum optomechanics in the unresolved sideband regime. Ph.D. thesis (2017).
48. Morsch, O. & Oberthaler, M. Dynamics of bose-einstein condensates in optical lattices. *Rev. Mod. Phys.* **78**, 179 (2006).
49. Maschler, C. & Ritsch, H. Quantum motion of laser-driven atoms in a cavity field. *Opt. Commun.* **243**, 145–155 (2004).
50. Domokos, P., Horak, P. & Ritsch, H. Semiclassical theory of cavity-assisted atom cooling. *J. Phys. B: At. Mol. Opt. Phys.* **34**, 187 (2001).
51. Nagy, D., Domokos, P., Vukics, A. & Ritsch, H. Nonlinear quantum dynamics of two bec modes dispersively coupled by an optical cavity. *Eur. Phys. J. D* **55**, 659–668 (2009).

52. Qu, K. Coherent interference effects and squeezed light generation in optomechanical systems. Ph.D. thesis, Oklahoma State University (2015).
53. Ritter, S. *et al.* Dynamical coupling between a bose-einstein condensate and a cavity optical lattice. *Appl. Phys. B* **95**, 213–218 (2009).
54. Brennecke, F., Ritter, S., Donner, T. & Esslinger, T. Cavity optomechanics with a bose-einstein condensate. *Science* **322**, 235–238 (2008).
55. Bergman, H. G., Bellman, R. & Kalaba, R. E. *Selected Papers on Mathematical Trends in Control Theory* (Dover Publications, 1964).
56. Peng, B., Özdemir, ŞK., Chen, W., Nori, F. & Yang, L. What is and what is not electromagnetically induced transparency in whispering-gallery microcavities. *Nat. Commun.* **5**, 1–9 (2014).
57. Wen, J., Dan, Y., Ma, X., Xu, L. & Sun, P. Frequency measurement and amplification of lidar echo signal based on optomechanical effects. *Opt. Continuum* **1**, 261–270 (2022).
58. Levitan, B., Metelmann, A. & Clerk, A. Optomechanics with two-phonon driving. *New J. Phys.* **18**, 093014 (2016).
59. Motazedifard, A., Dalafi, A., Naderi, M. & Roknizadeh, R. Controllable generation of photons and phonons in a coupled bose-einstein condensate-optomechanical cavity via the parametric dynamical casimir effect. *Ann. Phys.* **396**, 202–219 (2018).
60. Motazedifard, A., Dalafi, A., Naderi, M. & Roknizadeh, R. Strong quadrature squeezing and quantum amplification in a coupled bose-einstein condensate-optomechanical cavity based on parametric modulation. *Ann. Phys.* **405**, 202–219 (2019).
61. Motazedifard, A., Dalafi, A., Bemani, F. & Naderi, M. Force sensing in hybrid bose-einstein-condensate optomechanics based on parametric amplification. *Phys. Rev. A* **100**, 023815 (2019).
62. Motazedifard, A., Dalafi, A. & Naderi, M. Ultraprecision quantum sensing and measurement based on nonlinear hybrid optomechanical systems containing ultracold atoms or atomic bose-einstein condensate. *AVS Quant. Sci.* **3**, 024701 (2021).
63. Fani, M. & Dalafi, A. Back-action evading measurement of the collective mode of a bose-einstein condensate. *JOSA B* **37**, 1263–1272 (2020).
64. Scarlatella, O., Clerk, A. A. & Schiro, M. Spectral functions and negative density of states of a driven-dissipative nonlinear quantum resonator. *New J. Phys.* **21**, 043040 (2019).
65. Ban, M., Kitajima, S., Arimitsu, T. & Shibata, F. Linear response theory for open systems: Quantum master equation approach. *Phys. Rev. A* **95**, 022126 (2017).
66. Motazedifard, A., Dalafi, A. & Naderi, M. A green's function approach to the linear response of a driven dissipative optomechanical system. *J. Phys. A: Math. Theor.* **54**, 215301 (2021).
67. Askari, B. & Dalafi, A. Dynamics of a hybrid optomechanical system in the framework of the generalized linear response theory. *J. Phys. A: Math. Theor.* **55**, 035301 (2021).
68. Shen, H., Li, D. & Yi, X. Non-markovian linear response theory for quantum open systems and its applications. *Phys. Rev. E* **95**, 012156 (2017).

Author contributions

The authors' contributions in this work are as follows: H. M. carried out the analytical investigation, derived the first version of graphs, and provided the draft of the manuscript with help of the other authors. A. D. conceptualized and supervised the whole work, checked the results, and participated in writing and editing. M. G. contributed in design of the work, checking the results, writing, and editing. B. A. worked on numerical calculations, provided the computational codes, and created the final results.

Competing interests

The authors declare no competing interests.

Additional information

Correspondence and requests for materials should be addressed to A.D.

Reprints and permissions information is available at www.nature.com/reprints.

Publisher's note Springer Nature remains neutral with regard to jurisdictional claims in published maps and institutional affiliations.